Thermal conductivity of simple and tubular nanowire composites in the longitudinal direction

Ronggui Yang* and Gang Chen
Mechanical Engineering Department, Massachusetts Institute of Technology, Cambridge, Massachusetts 02139, USA

Mildred S. Dresselhaus
Department of Physics and Department of Electrical Engineering and Computer Science, Massachusetts Institute of Technology, Cambridge, Massachusetts 02139, USA

(Received 29 March 2005; published 13 September 2005)

This work establishes a generic model to study phonon transport and the thermal conductivity of periodic two-dimensional nanocomposites in the longitudinal direction (along the wire axis direction). More specifically, the generic model is applied to study the thermal conductivity of silicon-germanium composites with simple silicon nanowire and tubular silicon nanowire inclusions in a germanium matrix, and cylindrical nanoporous silicon materials. The results show that the effective thermal conductivity changes not only with the volumetric fraction of the constituents but also with the radius of the nanowires and cylindrical pores due to the nature of the ballistic phonon transport. The smaller the wire/pore diameter, the smaller is the thermal conductivity of the periodic two-dimensional nanocomposites for a given volumetric fraction. Composites with tubular nanowire inclusions have a lower effective thermal conductivity than simple nanowire composites due to the introduction of additional surface scattering through the pores associated with tubular nanowires. Results of this study can be used to direct the development of both high-efficiency thermoelectric materials and thermal interface material containing high-thermal-conductivity particle or wire inclusions.

DOI: 10.1103/PhysRevB.72.125418 PACS number(s): 68.65.−k, 44.10.+i, 63.22.+m

I. INTRODUCTION

Nanocomposite and nanoporous materials are used in a variety of applications and will play more important roles in the future with rapid progress being made in making controllable nanostructures, such as nanowires, nanotubes, and nanoparticles.[1] Thermal properties of nanocomposites are important for applications of particle-laden polymers in microelectronics as thermal interface materials[2,3] and nanoporous materials for sensor development.[4,5] Our interests in the thermal conductivity of nanocomposites arise from their potential applications in high efficiency thermoelectric materials.[6,7] The efficiency and energy density of thermoelectric devices are determined by the dimensionless thermoelectric figure of merit of the thermoelectric materials $ZT = S^2\sigma T/k$, where S is the Seebeck coefficient, σ is the electrical conductivity, k is the thermal conductivity, and T is the absolute temperature.[8] Significant advances for increasing ZT have been made, based on new ideas on how to engineer electron and phonon transport.[9] Nanocomposites may achieve high ZT through a thermal conductivity reduction while maintaining essentially the same electron transport performance.[7]

There are not many theoretical studies on the thermal conductivity of nanocomposites despite its importance for practical applications. The prevailing approach is to include the interface thermal resistance, or Kapitza resistance,[10] with the Fourier heat conduction theory.[11–15] However, Fourier heat conduction theory is based on the diffusion picture and is not applicable when the phonon mean free path is longer than the characteristic length of the nanocomposites such as the particle diameter and/or interparticle separation distance. Another approach in the investigation of the nanocomposite thermal conductivity is through the calculation of the phonon dispersion in periodic structures[16] Due to the short wavelength of the dominant phonon heat carriers, the phonon scattering at interfaces is often diffuse.[17] The diffuse interface scattering inside the nanostructure materials cannot only reduce the phonon mean free path but can also destroy the coherence of phonons. Due to the loss of coherence, classical size effect models such as the phonon Boltzmann equation are expected to be applicable to a wide range of nanostructures. In our previous article, the phonon Boltzmann equation is applied to study the classical size effect on the thermal conductivity of periodic nanowire composites (two-dimensional composites) normal to the wire axis direction.[7] In this article, we study the thermal conductivity of periodic two-dimensional nanocomposites with simple nanowire and tubular nanowire inclusions, and cylindrical nanoporous materials in the longitudinal direction, i.e., along the wire axis direction.

II. THEORETICAL MODEL AND NUMERICAL SIMULATION

In Fig. 1(a), a temperature gradient is applied along the axial direction (z direction) on a periodic two-dimensional nanocomposite with tubular nanowire inclusions. Since the transport is periodic in both x and y directions, the transport inside the nanocomposites can be represented by that in the small unit cell shown in Fig. 1(b) applying the totally specular phonon reflection boundary conditions along the x and y boundaries. However simulation of phonon transport in a 3-D unit cell shown in Fig. 1(b) is still a big challenge that involves both Cartesian and cylindrical coordinates. As an approximation, we further convert the outer surface of the square unit cell into a circle, i.e., to approximate a square

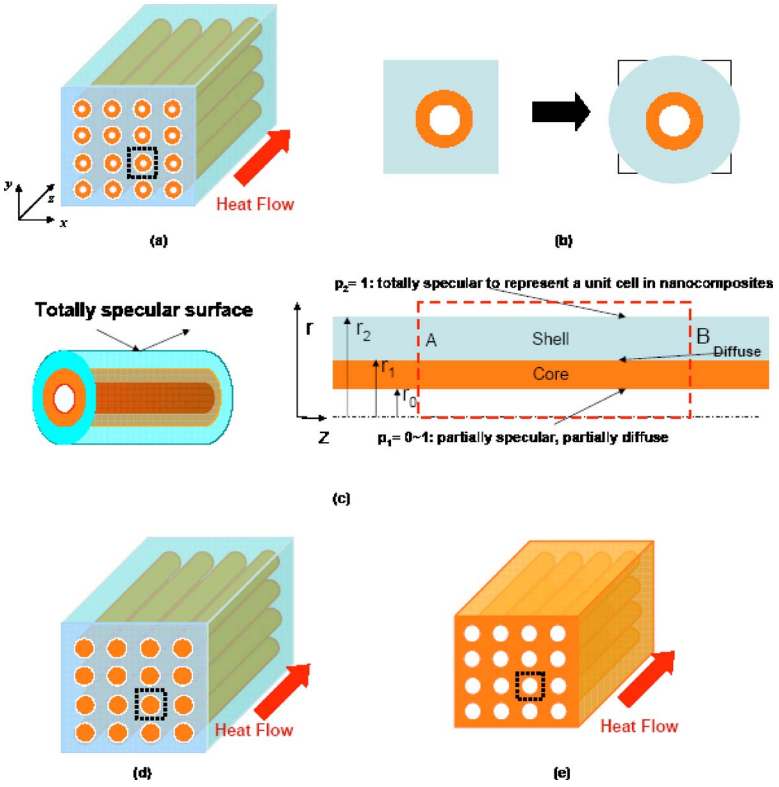

FIG. 1. (Color online) (a). Periodic two-dimensional nanocomposite (composite with tubular nanowire inclusions); (b) cross-sectional view of a unit cell: a square unit cell cross section is approximated as a circular cross section; (c) by the approximation in (b), the transport in nanocomposites becomes phonon transport in core-shell cylindrical structures; (d) periodic silicon nanowire composites; and (e) cylindrical nanoporous silicon material.

unit cell cross section as a circular cross section, as is often used to study fluid flow problems.[18,19] The problem then becomes phonon transport in core-shell cylindrical structures, as shown in Fig. 1(c). This approximation results in a 10% error. Figure 1(c) shows the generic phonon transport model we developed for core-shell nanostructures, which consists of a tubular core layer and a shell layer. Here we use the following notations: r_0 is the inner radius of the core layer, r_1 is the outer radius of the core layer, and r_2 is the outer radius of the shell. We assume partially diffuse and partially specular surface scattering at the inner surface of the core layer and totally specular reflection at the outer surface of the shell layer, to be consistent with what occurs at the outer surface of the unit cell shown in Fig. 1(b), i.e., to represent the phonon transport in nanocomposites. The specularity parameter at the inner surface of the core layer and the outer surface of the shell layer is represented by p_1 and p_2, respectively, where p $(=p_1$ or $p_2)=0$ corresponds to diffuse scattering and $p=1$ corresponds to specular scattering at the surface. This generic model can be used to simulate a variety of nanocomposites by changing some of the input parameters. For example, when the inner radius of the tubular core layer $r_0=0$ and the interface specularity $p_1=1$ at $r_0=0$, the structure represents periodic two-dimensional composites with simple wire inclusions as shown in Fig. 1(d). When the same material is used for the core and the shell layers, the interface between the core and shell layers disappears and the interface scattering at r_1 dies out; the model represents the phonon transport inside a nanoporous medium with cylindrical pores along the pore direction as shown in Fig. 1(e).

Clearly the model developed here is strictly valid for periodic composites only. In reality most of composites made might have random microstructures. Our study using Monte Carlo simulation shows that the thermal conductivity of a random nanocomposite is very close to a periodic composite.[20] In addition, the phonon Boltzmann transport model is based on the following assumptions: (1) the phonon wave effect can be excluded; (2) the frequency-dependent scattering rate in the bulk medium can be approximated by using an average phonon mean free path (MFP) Λ. Assumption (1) can be well justified since the wavelength for dominant phonons responsible for thermal transport is around 1 nm. The justification for these assumptions can be found in Refs. 7 and 21. In our simulation, we used the phonon MFP and the group velocity v listed in Ref. 21, which are obtained by approximating the dispersion of the transverse and the longitudinal-acoustic phonons with simple sine functions and neglecting the optical phonon contribution to the thermal conductivity k. This estimation leads to longer mean free path than using simple kinetic theory expression $k=\frac{1}{3}Cv\Lambda$, which is consistent with experiments from Goodson's group.[22]

In terms of the total phonon intensity I,[23,24] the 2-D phonon Boltzmann equation under the single mode relaxation time approximation in cylindrical coordinates can be written as

$$\frac{\mu}{r}\frac{\partial}{\partial r}(rI_i) - \frac{1}{r}\frac{\partial}{\partial \phi}(\eta I_i) + \zeta\frac{\partial I_i}{\partial z} = -\frac{I_i - I_{oi}}{\Lambda_i}, \qquad (1)$$

where subscript i $(=1,2)$ denotes properties of the core and shell material Λ_i is the average phonon MFP. μ, η, and ζ are the directional cosines defined as

$$\mu = \sin\theta\cos\phi, \quad \eta = \sin\theta\sin\phi, \quad \zeta = \cos\theta, \qquad (2)$$

where θ and ϕ are the polar and azimuthal angles, respectively, as shown in Fig. 2. In the phonon Boltzmann transport

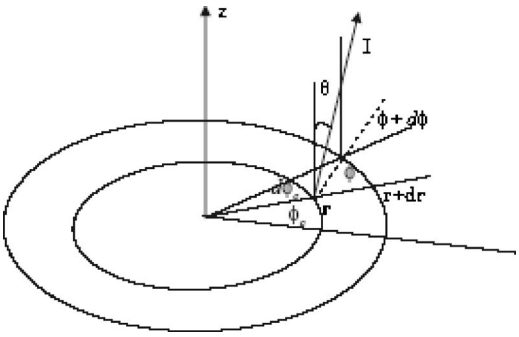

FIG. 2. Phonon transport in cylindrical coordinate.

equation [Eq. (1)], there are two coordinate systems [shown in Fig. 2]: spatial coordinates (r, ϕ_c, and z) and directional coordinates (θ and ϕ) for the transport, which correspond to the movement of carriers in spatial and momentum space. As a phonon travels through a curved geometry such as in the cylindrical coordinates, the propagating direction is constantly varying, even though the phonon does not physically change its direction. This is why an additional term, the second term of the left-hand side in Eq. (1), exists. The difficulty of numerical simulation is also due to this term. There exist many procedures to address this term in the neutron transport literature.[25] I_{oi} in Eq. (1) is determined by the Bose-Einstein distribution of phonons and depends on the local equilibrium temperature. In nanostructures, local equilibrium cannot be established and thus the temperature obtained should not be treated in the same way as in the case of local thermal equilibrium. An energy balance shows that I_{oi} can be calculated from[26]

$$I_{oi}(r,z) = \frac{1}{4\pi}\int_{4\pi} I_i(r,\Omega)d\Omega = \frac{1}{4\pi}\int_0^{2\pi}\int_0^{\pi} I_i(r,z,\theta,\phi)\sin\theta d\theta d\phi \qquad (3)$$

and the corresponding temperature obtained is a measure of the local energy density.

Equation (1) is similar to the photon radiative transport equation (RTE).[26] The key is to solve for the intensity distribution $I(r,\Omega)$. A variety of solution methods are available in the thermal radiative transfer literature.[25,27] For phonon transport in nanostructures, the challenge is to reduce the "ray effect," which often happens similarly in thermal radiation in optical thin limit. In our previous work,[28] double Gauss-Legender quadratures have been used to replace the conventional S_N quadratures for the discrete ordinate method and this approach was shown to successfully resolve the ray effect problem in our phonon transport simulation in nanostructures. In the present work, we extend the previous work in Cartesian coordinates to cylindrical coordinates. The method separately discretizes the integrating points in $\zeta = \cos\theta$ (the angle θ) and in the angle ϕ using the Gauss-Legender quadrature. To obtain high accuracy, μ is discretized into 120 points from -1 to 1 and ϕ is discretized into 24 points for 0 to π (not 0 to 2π due to symmetry). Then Eq. (3) can be written in discrete form as

$$I_{0i}(r,z) = \frac{2}{4\pi}\sum_m \sum_n I_i(r,z,\zeta_n,\phi_m)w_n w'_m. \qquad (4)$$

The weights w_n and w'_m satisfy $\Sigma_m \Sigma_n w_n w'_m = 2\pi$.

Following the conventional artifice of Carlson and Lathrop[25] and Lewis and Miller,[29] which maintain phonon radiative energy conservation and permits minimal directional coupling, the angular derivative term can be written as follows:

$$\frac{\partial}{\partial\phi}(\eta^{nm} I_i^{nm}) = \frac{\alpha_{n,m+1/2} I_i^{n,m+1/2} - \alpha_{n,m-1/2} I_i^{n,m-1/2}}{w_n w'_m}, \qquad (5)$$

where $w_n w'_m$ is a weight and $\alpha_{n,m\pm1/2}$ is the coefficient for the angular derivative term determined from the nondivergent flow condition as following the recursive equation:

$$\alpha_{n,m+1/2} - \alpha_{n,m-1/2} = (w_n w'_m)\mu^{n,m}. \qquad (6)$$

For this work, we are only interested in the size effect occurring in the radial direction, not in the wire axis direction. However, because heat flows along the axial direction, the simulation requires choosing a proper length and the corresponding boundary conditions at the two ends along the transport direction. When heat is enforced to flow in the axial direction, the temperature is different in the two ends. However, simply assuming the temperature difference in the two ends might induce artificial size effect in the axial direction. To get rid of the artificial size effect in the axial direction, the periodic boundary condition on the phonon distribution deviation proposed in our earlier work[7] is used. This periodic boundary condition requires that the deviation of phonon intensity in each direction at each point in one boundary is the same as the deviation in the corresponding point and direction in the other boundary of the simulation domain in the heat transport direction. The equation can be expressed as

$$I(r,L_Z,\theta,\phi) - I_0(r,L_Z) = I(r,0,\theta,\phi) - I_0(r,0), \qquad (7)$$

where L_Z is the simulation domain length. It can be proved that the temperature difference between the two ends should be independent of r and can be related to

$$I_o(r,L_Z) - I_o(r,0) = \frac{C_i v_i[T(r,L_Z) - T(r,0)]}{4\pi} = \text{const}. \qquad (8)$$

In our simulation, we superimposed $T(r,L_Z) - T(r,0) = 1$ K in the above equation. If we do not superimpose such a temperature difference in the program, Eq. (7) will automatically converge to a constant temperature difference $T(r,L_Z) - T(r,0)$ value. The converged value varies with simulated structures. But the final results of the thermal conductivity value do not depend on whether the temperature difference is superimposed. However, the calculation is much faster when the temperature difference value is superimposed. Other than the temperature difference shown in Eq. (8), Eq. (7) is apparently a more demanding boundary condition, which ensures directional heat flux conservation in the two boundaries along the transport direction. For trans-

port along the axial direction, the periodicity is arbitrary. So we can choose an arbitrary length L_Z and use the periodic boundary condition to obtain thermal conductivity values that are independent of L_Z. If the boundary conditions at the two ends are assumed as emitted temperature condition,[28] one often needs to simulate a domain more than three times longer than the phonon mean free path, which can be many times longer than the size in the radial direction. With the proposed boundary condition, the simulation domain length can be adjusted according to the size of the structure in the radial direction. We also note that the nature of the Boltzmann equation requires iterations to obtain convergent results with the boundary conditions we have defined.

As in previous work, a nonuniform grid system and the step scheme is used for spatial discretization to accurately capture the physics of the transport phenomena and to minimize the calculation time. The step scheme is used for spatial discretization. The equation is solved by iteration over the value of the equivalent equilibrium intensity $I_{0i}(r,z) = (2/4\pi)\Sigma_m \Sigma_n I_i(r,z,\zeta_n,\phi_m) w_n w'_m$. Assuming constant specific heat over a wide temperature range, we can write effective temperature, which is a measure of the local energy density inside the medium, as

$$T(r,z) = \frac{4\pi I_0(r,z)}{C_i |v_i|}. \tag{9}$$

The heat flux along the axial direction at every point can be accordingly written as

$$q_z(r,z) = \sum_m \sum_n I(x,y,\zeta_n,\phi_m)\zeta_n w_n w'_m, \tag{10}$$

The surface heat flux in the axial direction can be calculated as

$$Q_z(z) = \int_0^{r_2} q_z(r,z) 2\pi r dr. \tag{11}$$

When the simulation is converged, $Q_z(z) = \text{const}$. After local effective temperature distribution and heat flux are obtained, the thermal conductivity calculation is straightforward. The effective thermal conductivity k of the core-shell structure can be obtained as

$$k = \frac{Q_z L_Z}{\pi r_2^2 [T(r,L_Z) - T(r,0)]}. \tag{12}$$

III. RESULTS AND DISCUSSIONS

Figure 3 shows results for the thermal conductivity of a silicon-germanium nanocomposite which consists of a germanium matrix with silicon wire inclusions [as shown in Fig. 1(d)] as a function of the silicon wire radius and the volumetric ratio of Si, $\Phi_{Si} = {r_1}^2/{r_2}^2$, which can be related to the atomic ratio γ_{Si} through $\gamma_{Si} = \Phi_{Si}/[\Phi_{Si} + (1-\Phi_{Si})a_{si}/a_{Ge}]$, where a is the lattice constant. The phonon scattering at the silicon-germanium interface is assumed to be diffuse and the phonon transmissivity at the interface can be calculated as[30]

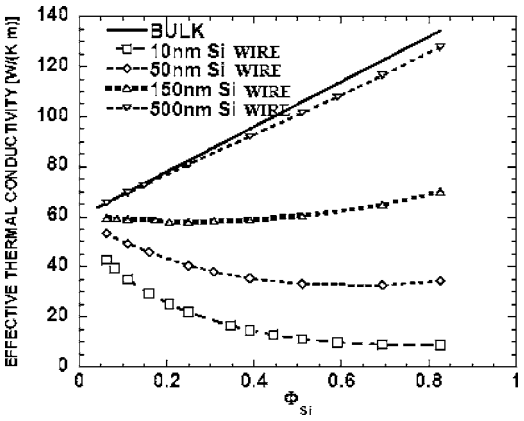

FIG. 3. Thermal conductivity of silicon germanium nanocomposite which is comprised of a germanium matrix with silicon wire inclusions as a function of the silicon wire radius and the volumetric ratio.

$$T_{d12}(T) = \frac{U_2(T)v_2}{U_1(T)v_1 + U_2(T)v_2}, \tag{13}$$

where U is the volumetric internal energy. In a bulk Si-Ge composite, the effective thermal conductivity increases linearly as the cross-sectional area or volumetric ratio of Si (Φ_{Si}) increases since Si has much higher thermal conductivity than Ge. For Si-Ge nanocomposites, the effective thermal conductivity decreases as the radius of wire inclusion decreases due to the relative increasing interface scattering area per unit volume. When the radius of the wire inclusion is larger than 500 nm, the effective thermal conductivity approaches asymptotically that of macroscale composites. This means that the interface scattering is negligible compared to the internal thermal resistance in Si wires and the Ge matrix and the effective value can be predicted by the Fourier law. For nanowire composites with the wire inclusion radius less than 150 nm, there exists a minimum thermal conductivity as the volumetric ratio of Si changes. The trend is similar as those predicted for core-shell Si-Ge nanowires. When the volumetric ratio of Si (Φ_{Si}) in the composites is large, the effective thermal conductivity has the same trend as that of the macroscale composite. When the volumetric ratio of Si (Φ_{Si}) in the composites is small, the effective thermal conductivity increases as the fraction of the low thermal conductivity component increases, which is contrary to the behavior of bulk composites. This is because the effective thermal conductivity of the Si wire k_{eSi} is decreased to well below the bulk Ge thermal conductivity due to interface scattering. The effective thermal conductivity of the Ge matrix k_{eGe} increases as $(r_2 - r_1)/r_1$ increases, since the scattering surface per unit volume of Ge decreases. The effective thermal conductivity of the core-shell structure can be written as $[k^*_{eSi} {r_1}^2 + k^*_{eGe}({r_2}^2 - {r_1}^2)]/{r_2}^2$, thus accounting for the existence of a minimum value.

As stated in the Introduction, most past studies on the thermal conductivity of nanocomposites were based on the Fourier diffusion theory together with consideration of the thermal boundary resistance. To examine the validity of such

an approach, we compare the effective thermal conductivity obtained from the Boltzmann equation with that of the effective medium approach (EMA) developed by Nan *et al.*, which gives the anisotropic effective thermal conductivity values of nanowire composites as[13]

$$k_{11} = k_{22} = k_m \frac{k_P(1+\alpha) + k_m + \Phi_P[k_P(1-\alpha) - k_m]}{k_P(1+\alpha) + k_m - \Phi_P[k_P(1-\alpha) - k_m]}, \tag{14}$$

$$k_{33} = (1-\Phi_P)k_m + \Phi_P k_P, \tag{15}$$

where k_{11} and k_{22} are the effective composite thermal conductivity across the wire axis direction, k_{33} is the effective thermal conductivity in the longitudinal direction, k_m is the thermal conductivity of the host material, k_P is the bulk thermal conductivity of the nanowire inclusion materials, Φ_P is the volume fraction of nanowire inclusion, and α is a dimensionless parameter defined as $a=a_k/a_p$ for nanowire composites. a_p is the radius of nanowire inclusions and $a_k=Rk_m$, where R is the interface thermal resistance which can be calculated as[21]

$$R = \frac{4}{T_{d12}U_1 v_1} \approx \frac{4(U_1 v_1 + U_2 v_2)}{U_1 v_1 U_2 v_2}. \tag{16}$$

Apparently, Eq. (15) shows that the EMA model does not consider the size effect on the thermal conductivity for nanowire composites in longitudinal direction, i.e., when the temperature gradient is applied along the wire axis direction. Such a result is clearly contrary to the solution of the Boltzmann equation presented above that shows a strong size dependence. We further compare k_{11}, the thermal conductivity perpendicular to the wire axis, with our previous calculations.[7] As our previous calculation was done for square wire inclusions, an effective diameter $D=2a_p=4A_C/P$ is used, where A_C is the cross-sectional area and P is the perimeter of the cross section, to convert the square geometry into a circular geometry. Figure 4 compares the thermal conductivity in nanowire composites perpendicular to wire axis obtained from the phonon Boltzmann equation simulation and the effective medium approximation (EMA). As we can see, the effective medium approach based on incorporating the thermal boundary resistance into the solutions of the Fourier heat conduction law leads to erroneous results that underpredict the size effects.

The same code can be used to simulate the thermal conductivity of a nanoporous medium. Figure 5 shows results for the thermal conductivity of porous silicon along the cylindrical pore direction [as shown in Fig. 1(e)]. Here r_0 is the pore radius and the shell thickness (r_2-r_0) is determined by the porosity as $\Phi_o=r_0^2/r_2^2$. For simplicity, only the results assuming diffuse surface scattering at the pore surface are reported. For macroscale porous materials, the effective thermal conductivity decreases linearly as the porosity increases. When the pore radius is less than two to three times the phonon mean free path in the silicon matrix, the effective thermal conductivity is not only a function of porosity, but also a function of pore radius. For composites with the same porosity, the effective thermal conductivity decreases as the pore radius decreases since the scattering area per unit volume increases. The implication of this study is that nanopores can possibly be used to further reduce the thermal conductivity of nanowire composites. In a recent report, Zhao *et al.* showed that the effective thermal conductivity is further reduced and thus the thermoelectric figure of merit ZT is increased in a Bi_2Te_3 composite with tubular Bi_2Te_3 nanowire inclusions.[31]

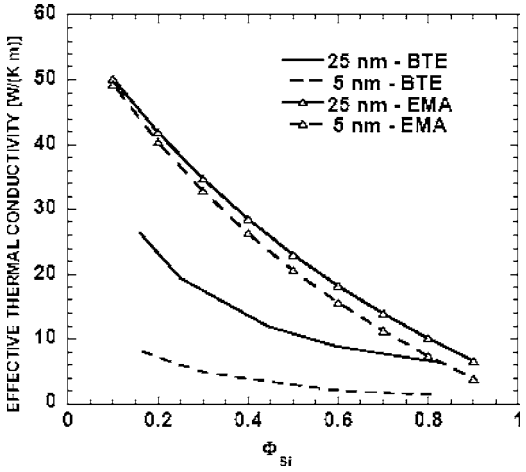

FIG. 4. Comparison of the thermal conductivity of nanowire composites in the direction perpendicular to the wire axial direction obtained from phonon Boltzmann equation simulation and from the effective medium approximation (EMA) based on the Fourier law and thermal boundary resistance, demonstrating that the EMA underpredicts size effects.

The model has also been used to study the thermal conductivity of tubular nanowire composites as shown in Fig. 1(a). Again the results shown here assume a totally diffuse surface scattering at the pore surface. The effective thermal conductivity of tubular nanowire composites is a function of the pore radius inside the tubular silicon wire r_0, the outer radius of the silicon shell r_1 (silicon shell thickness is defined as r_1-r_0), and the volumetric ratio of silicon $\Phi_{Si}=(r_1^2-r_0^2)/(r_2^2-r_0^2)$ in the composites. Figure 6 shows the effect of the silicon core layer thickness of the tubular

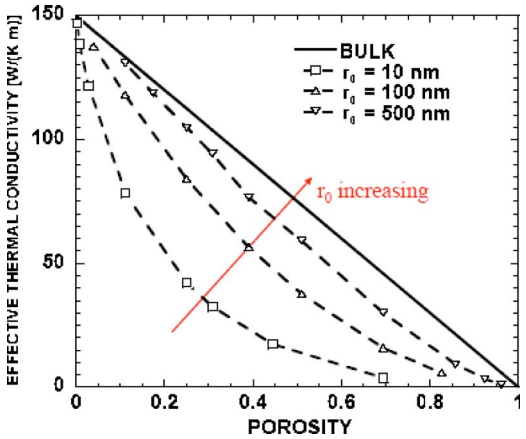

FIG. 5. (Color online) Thermal conductivity of porous silicon along the cylindrical pore direction as a function of the pore radius and porosity.

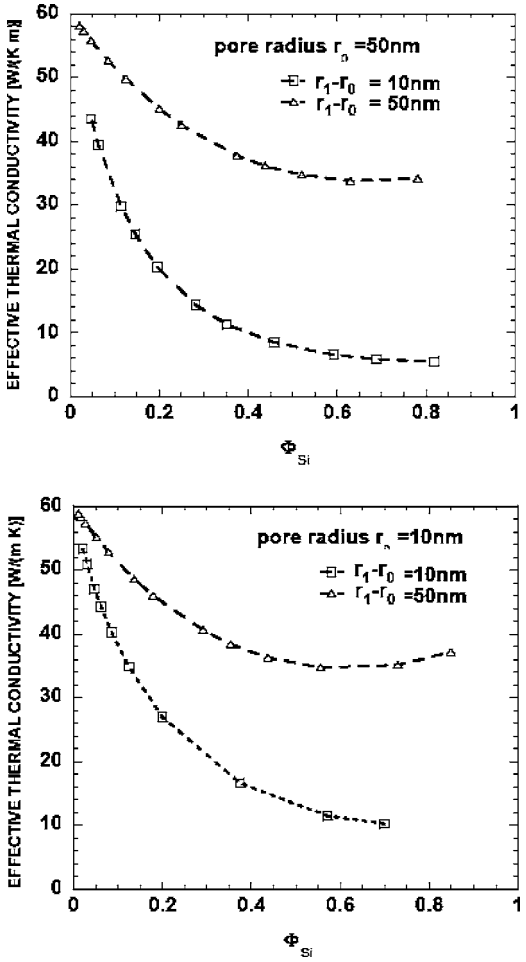

FIG. 6. The effect of the silicon core layer thickness and the pore size of tubular silicon wire inclusions on the effective thermal conductivity of the nanocomposites.

silicon wire inclusions on the effective thermal conductivity of the nanocomposites. From Fig. 6, the effective thermal conductivity is smaller when the Si core layer thickness is thinner for the same volumetric ratio of Si and same inner pore radius. A smaller Si shell thickness means smaller Ge shell thickness. This gives a smaller effective thermal conductivity for both the Si and Ge layers and thus a smaller effective thermal conductivity of the nanocomposites. Comparison of Figs. 6(a) and 6(b) shows that the effective thermal conductivity of the composites decreases as the radius of the inner pores increases for fixed Si shell thickness and volumetric ratio of Si due to the increase of surface scattering area per unit volume.

Figure 7 shows that the tubular Si nanowire composite has lower solid thermal conductivity than that of simple nanowire composite due to the additional surface scattering introduced through the inner pore surface. Here the solid thermal conductivity k_S is defined as $k_S = QL/A_S\Delta T$, where Q is the heat flux, L is the length of the simulation domain along the direction where the temperature difference ΔT is applied, and A_S is the solid part of the cross-sectional area

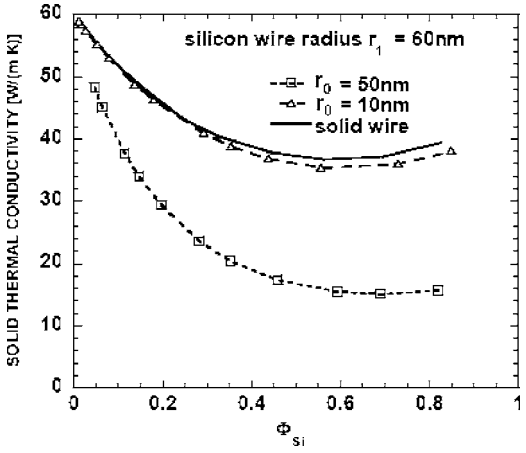

FIG. 7. The solid thermal conductivity of the composites decreases as the pore radius increases due to the increasing surface scattering per unit volume.

$A_s = \pi(r_2^2 - r_0^2)$. For comparison, the Si wire radius (or outer shell radius of the tubular nanowire) is fixed. Figure 7 also shows that the solid thermal conductivity decreases as the pore radius increases due to the increasing surface scattering per unit volume.

IV. CONCLUSION

We study in this paper the thermal conductivity of periodic two-dimensional nanocomposites along the wire axis direction, including simple nanowire composites, nanoporous medium, and composites with tubular nanowire inclusions. The results show that the effective thermal conductivity changes not only with the volumetric fraction of the constituents but also the radius of the nanowire, pore, and tubular nanowire inclusions due to the nature of the ballistic phonon transport. These results are in contradiction with the existing theory on the thermal conductivity of composites, which lead to effective transport properties depending only on the volume fraction but independent of size. The smaller the wire/pore diameter, the smaller is the thermal conductivity of periodic two-dimensional nanocomposites for a given volumetric fraction. Composites with tubular nanowire inclusions have both lower effective and solid thermal conductivity than simple nanowire composites due to the introduction of surface scattering through the pores. We also show that the effective medium approach based on incorporating the thermal boundary resistance into the solution based on the Fourier heat conduction law leads to erroneous results that underpredict the size effects. Results of this study can be used to direct the development of both high efficiency thermoelectric materials and thermal interface materials with high thermal conductivity particle or wire inclusions.

ACKNOWLEDGMENTS

The work is financially supported by NASA Contract No. NAS3-03108.

*Also at Department of Mechanical Engineering, University of Colorado, Boulder, Colorado 80309, USA.

[1] Y. N. Xia, P. D. Yang, Y. G. Sun, Y. Y. Wu, B. Mayers, B. Gates, Y. D. Yin, F. Kim, and Y. Q. Yan, Adv. Mater. (Weinheim, Ger.) **15**, 353 (2003); M. Law, J. Goldberger, and P. D. Yang, Annu. Rev. Mater. Res. **34**, 83 (2004).

[2] A. R. Abramson, W. C. Kim, S. T. Huxtable, H. Tan, Y. Wu, A. Majumdar, C.-L. Tien, and P. Yang, J. Microelectromech. Syst. **13**, 505 (2004).

[3] R. S. Prasher, J. Shipley, S. Prastic, P. Koning, and J. L. Wang, J. Heat Transfer **125**, 1170 (2003).

[4] V. Lysenko, S. Perichon, B. Remaki, D. Barbier, and B. Champagnon, J. Appl. Phys. **86**, 6841 (1999).

[5] A. Drost, P. Steiner, H. Moser, and W. Lang, Sens. Mater. **7**, 111 (1995).

[6] G. Chen, Semicond. Semimetals **71**, 2003 (2001).

[7] R. G. Yang and G. Chen, Phys. Rev. B **69**, 195316 (2004).

[8] H. J. Golsmid, *Thermoelectric Refrigeration* (Plenum Press, New York, 1964).

[9] T. M. Tritt, ed., Semicond. Semimetals 69–71 (2001).

[10] P. L. Kapitza, J. Phys. **4**, 181 (1941); E. T. Swartz and R. O. Pohl, Rev. Mod. Phys. **61**, 605 (1989).

[11] D. P. H. Hasselman and L. F. Johnson, J. Compos. Mater. **21**, 508 (1987).

[12] Y. Benvensite, J. Appl. Phys. **61**, 2840 (1987); Y. Benvensite and T. Miloh, *ibid.* **69**, 1337 (1991).

[13] C.-W. Nan, R. Birringer, D. R. Clarke, and H. Gleiter, J. Appl. Phys. **81**, 6692 (1997); C.-W. Nan, Z. Shi, and Y. Lin, Chem. Phys. Lett. **375**, 666 (2003).

[14] J. D. Felske, Int. J. Heat Mass Transfer **47**, 3453 (2004).

[15] S. Y. Lu and J. L. Song, Chem. Eng. Sci. **51**, 4393 (1996).

[16] O. L. Lazarenkova and A. A. Balandin, J. Appl. Phys. **89**, 5509 (2001); Phys. Rev. B **66**, 245319 (2002); A. A. Balandin and O. L. Lazarenkova, Appl. Phys. Lett. **82**, 415 (2003).

[17] B. Yang and G. Chen, Phys. Rev. B **67**, 195311 (2003).

[18] J. A. Fay, *Introduction to Fluid Mechanics* (MIT Press, Cambridge, MA, 1994).

[19] J. H. Lienhard, *A Heat Transfer Textbook*, http://web.mit.edu/lienhard/www/ahtt.html (2005).

[20] M. S. Jeng, R. G. Yang, and G. Chen, Phys. Rev. B (to be published).

[21] G. Chen, Phys. Rev. B **57**, 14958 (1998).

[22] K. E. Goodson and Y. S. Ju, Annu. Rev. Mater. Sci. **29**, 261 (1999).

[23] A. Majumdar, J. Heat Transfer **115**, 7 (1993).

[24] G. Chen and C. L. Tien, J. Thermophys. Heat Transfer **7**, 311 (1993).

[25] *Computing Methods in Reactor Physics*, edited by H. Greenspan, C. N. Kelber, and D. Okrent (Gorden and Breach, London, 1967).

[26] A. A. Joshi and A. Majumdar, J. Appl. Phys. **74**, 31 (1993).

[27] M. F. Modest, *Radiative Heat Transfer*, 2nd ed. (Academic Press, New York, 2003).

[28] R. G. Yang, G. Chen, M. Laroche, and Y. Taur, J. Heat Transfer **127**, 298 (2005).

[29] E. E. Lewis and W. F. Miller, *Computational Method of Neutron Transport* (Wiley, New York, 1984), pp. 156–207.

[30] C. Dames and G. Chen, J. Appl. Phys. **95**, 682 (2004).

[31] X. B. Zhao, X. H. Ji, Y. H. Zhang, T. J. Zhu, J. P. Tu, and X. B. Zhang, Appl. Phys. Lett. **86**, 062111 (2005).